

# Cavity ring-down overtone spectroscopy of HCN, H<sup>13</sup>CN and HC<sup>15</sup>N

Daniele Romanini and Kevin K. Lehmann

Department of Chemistry, Princeton University, Princeton, New Jersey 08544

(Received 13 July 1994; accepted 5 October 1994)

This paper reports the results of our use of Cavity Ring Down Spectroscopy to extend the study of highly excited vibrational states in HCN. We extend our previous study of the H<sup>12</sup>C<sup>14</sup>N isotopomer, reporting on some weaker bands between 17 500 and 19 500 cm<sup>-1</sup>. We also report spectra of overtone and combination bands with six, seven, and eight quanta of stretching vibration in the isotopomers H<sup>12</sup>C<sup>15</sup>N and H<sup>13</sup>C<sup>14</sup>N in the interval from 17 500 to 23 000 cm<sup>-1</sup>. The observed spectroscopic constants and band intensities are compared with calculated values. All but one of the observed bands can be fit to within experimental accuracy (~0.02 cm<sup>-1</sup>) to the standard distortable-rotor Hamiltonian. The one perturbed band has been successfully analyzed in terms of three anharmonically coupled levels. An anomalous line intensity distribution has been observed in the 11<sup>1</sup>5 and 01<sup>1</sup>6  $\Pi \leftarrow \Sigma$  bands, which we believe is produced by Coriolis coupling. © 1995 American Institute of Physics.

## I. INTRODUCTION

The experimental investigation of highly excited molecular states provides information essential to characterizing both intramolecular dynamics and potential energy surfaces. Comparison of both experimental overtone transition energies and intensities with theoretical values provide complementary tests of *ab initio* and empirical potential energy surfaces.<sup>1</sup> The observable effects of coupling between quasi-separable modes, give information relevant to studies of intramolecular vibrational energy redistribution (IVR).

Extensive experimental data are available for the most common isotopomers of hydrogen cyanide. The lower vibrational states have been investigated by several authors.<sup>2-5</sup> Overtone spectra with up to six stretching quanta (up to 18 500 cm<sup>-1</sup>) have been thoroughly characterized using photoacoustic and White-cell absorption spectroscopies by Lehmann, Smith *et al.*<sup>6-10</sup> Diode laser spectra of the first CH stretch overtone have been reported by Sasada.<sup>11</sup> Yang, Rogaski, and Wodtke<sup>12-14</sup> used stimulated emission pumping (SEP) to study high overtones and combinations of the bending and the CN stretching modes. Carrasquillo *et al.*<sup>15</sup> have used collisional energy transfer from the 3  $\nu_3$  level to populate states dark in both overtone and SEP spectroscopies. We have previously reported on higher overtone transitions, with energy up to 23 000 cm<sup>-1</sup>, well above the isomerization barrier.<sup>16</sup> The present paper represents a continuation of that study.

As a result of increased sensitivity in the spectral region 17 500–19 500 cm<sup>-1</sup>, we have been able to detect some weaker H<sup>12</sup>C<sup>14</sup>N overtone bands, which we report in the present paper. We also report spectra of the isotopomers H<sup>12</sup>C<sup>15</sup>N and H<sup>13</sup>C<sup>14</sup>N in the spectral region from about 17 500 to 23 000 cm<sup>-1</sup>. Isotopic shifts, when viewed as a perturbation using the Hellmann–Feynman Theorem, give the kinetic energy of the substituted atom in the vibrational state. As such, they are direct measures of the distribution of vibrational energy in the molecule, and a sensitive test of the character of approximate vibrational wave functions. Due to poor control over the purity of the isotopically enriched

samples, we unfortunately did not determine accurate intensities for these isotopomers. For H<sup>13</sup>C<sup>14</sup>N we do report some estimated band intensities, but these should be considered as lower bounds for the real values, due to the unknown sample partial pressure. As with previously reported data, good agreement is found between our observed spectroscopic data and predicted band origins (Carter, Handy, and Mills, “CH&M”,<sup>17,18</sup>) and intensities (Peter Botschwina<sup>19</sup>).

In this paper, we use Hertzberg’s convention for numbering the vibrational modes of HCN since most of the literature has used these labels;  $\nu_1$  is the CN stretch,  $\nu_2$  the degenerate bending mode, and  $\nu_3$  the CH stretch. Many recent authors have inverted the numbering of the two stretching modes to be consistent with modern conventions. Also, in the following, we will refer to the three isotopomers more simply as HCN, H<sup>13</sup>CN and HC<sup>15</sup>N.

The experimental methods and much of the analysis have closely followed those discussed in our previous paper. One problem will be considered in detail. This concerns the analysis of the HC<sup>15</sup>N 206 band system, which is the only observed overtone band that cannot be fit to an effective Hamiltonian for a single vibrational level. We have found that the observed spectrum can be quantitatively fit to an effective Hamiltonian that contains three vibrational bands coupled by anharmonic interactions.

Another problem comes from the observation that the (11<sup>1</sup>5←000) band in HCN and H<sup>13</sup>CN, and the (01<sup>1</sup>6←000) band in H<sup>13</sup>CN are all characterized by an anomalous asymmetry in the line intensity of the *P* and *R* branches. This Herman–Wallis effect<sup>20,21</sup> is attributed to Coriolis mixing with  $\Sigma$  states possessing much larger transition strengths. We are presently trying to calculate this effect, which has also been observed in lower vibrational transitions in HCN.<sup>22</sup> This analysis will represent a further test of the quality of the available *ab initio* dipole moment surface for HCN.<sup>19</sup>

## II. EXPERIMENT

We have used a recently introduced technique<sup>23</sup> of cavity ring down spectroscopy (CRDS) to study very weak visible

overtone transitions of HCN and some of its isotopomers. The theory and our implementation of CRDS is described in detail in our previous paper<sup>16</sup> to which the reader is referred for details. This technique gives sensitivity comparable to intracavity photoacoustic spectroscopy with a continuous wave (cw) laser. CRDS uses pulsed lasers of much lower average power than the cw lasers required for photoacoustic spectroscopy at comparable sensitivity. CRDS is an absorption technique and directly gives spectra in absolute absorbance units. In our work, knowledge of sample concentration has been the limiting factor in the determination of absolute integrated band intensities.

A brief description of our experimental setup is as follows. An excimer-pumped dye laser is coupled into an optical cavity formed by a pair of high-reflective mirrors, which act as the input and output windows of our gas cell. Light from the dye laser strikes the front mirror, and a small fraction ( $\sim 10$  ppm) is transmitted into the optical cavity. The exponential decay ("ring-down") of the light intensity inside the cavity is monitored as the laser frequency is scanned. The effect of sample absorption is detected as a decrease in the time constant of the exponential decay when the laser is tuned into resonance with the molecular transition. The "effective" absorption pathlength can be defined in terms of this time constant. For high quality mirrors, we have observed decay time constants on the order of 100  $\mu$ s, which correspond to an effective absorption path-length of 60 km.

The performance of CRDS can be substantially degraded by the presence of impurities on the dielectric coating of the mirrors, such as dust or chemical deposits, that increase mirror loss and lower the effective pathlength of the cell. We have found,<sup>24</sup> that one has to be careful when evacuating the ring down cavity (RDC) and filling it with sample. If these operations are done too quickly, transitory condensation may occur which leaves the mirror surfaces dirty. We observed an improvement by a factor 3 of the ring down time in the range from 17 500 to 19 500  $\text{cm}^{-1}$  when the cell was slowly pumped before filling. We did not make a systematic study of this problem, and by "slowly" we mean a pumping time of 10 minutes to 1 hour. Unfortunately, we did not observe such a dramatic improvement when using mirrors coated for higher frequencies, perhaps due to their higher intrinsic loss.

The HCN samples used in this study were prepared by the reaction of KCN with stearic acid. The solids are mixed together and are nonreactive. The reaction bulb is then pumped down to less than 10 mtorr pressure. When the stearic acid is melted (around 71 °C) the reaction to produce HCN and potassium stearate proceeds slowly and to completion in a few hours. We used about a 2:1 stoichiometric excess of stearic acid. For production of both the  $\text{H}^{13}\text{CN}$  and  $\text{HC}^{15}\text{N}$  isotopomers, we used isotopically labeled KCN salts with reported isotopic purity of 90 and 97%, respectively. These salts were kindly provided by Dr. Alec Wodtke. Fourier transform infrared (FTIR) spectra of these HCN samples reveal impurities of  $\text{CO}_2$  and water, which were partially removed by cryotrapping.

Due to the incomplete purification and to the presence of other unknown impurities, the band intensities we obtained from the isotopomer samples were not very consistent (sys-

tematically smaller than the HCN values, in some cases by as much as 30%) and not very reproducible (as much as 10% variation between separate measurements).

However, the band intensities for the normal HCN reported here and in our previous paper, were remeasured using HCN cryotrapped from a 2% commercial mixture with He (by Matheson gases). These measurements yielded more consistent and repeatable results, allowing us to place an error bar of 10% on the reported band intensities. In view of these circumstances, we decided not to report the band intensities we measured in the isotopomers, except for a few bands for which we did not measure the corresponding band in the principal isotopomer. These intensities should be considered as lower bounds to the real values.

### III. DATA ANALYSIS

The data analysis was done using the same methods as described in our previous paper. The spectra were linearized in frequency by using etalon transmission peaks recorded during the laser scan. Line frequencies, linewidths, and integrated intensities were determined from a fit of the spectrum to a sum of Voigt line shapes. The fitting program is based on the Levenberg–Marquardt least-square minimization algorithm.<sup>25</sup> By an automatic scheme of toggling between fixed and floated parameters, the program is capable of producing excellent fits even in presence of strong line blending. For each band, the integrated band intensity  $S_0$  was obtained by averaging over the value calculated from all the strong and well-resolved lines.

The factors used to calculate  $S_0$  from the fitted line intensity and shape are given in Ref. 10. Physically,  $S_0$  is equal to Avogadro's number times the absorption cross section integrated over the band wave number. For the  $\Sigma \leftarrow \Sigma$  transitions, there was no significant Herman–Wallis correction to the line intensities. This correction results from rotation–vibration interactions. In the case of the very weak  $\Pi \leftarrow \Sigma$  transitions, we did find a substantial Herman–Wallis correction. For these bands, in the fit of  $S_0$  the individual line strengths are corrected by a factor of  $(1 + Am)^2$ , ( $m$  is  $-J$  in the  $P$  branch and  $J+1$  in the  $R$  branch) where  $A$  is the linear Herman–Wallis coefficient.

Note that the old convention was to define the correction factor as  $(1 + Am)$ , which gives twice the  $A$  coefficient for a weak Herman–Wallis effect.<sup>20,21</sup> The present formula, adopted by Watson,<sup>26</sup> gives reasonable intensities even for a strong Herman–Wallis effect, as observed in the  $\nu_1$  fundamental.<sup>22</sup> The band intensity and Herman–Wallis coefficient determined for each of the  $\Pi \leftarrow \Sigma$  bands have the following values:

Transition	$S_0(\text{cm/mol})$	$A$
HCN $11^15 \leftarrow 000$	0.0129(8)	0.0110(28)
$\text{H}^{13}\text{CN}$ $11^15 \leftarrow 000$	0.0073(4)	0.0086(24)
$\text{H}^{13}\text{CN}$ $01^16 \leftarrow 000$	0.0116(7)	0.0281(32)

The present results give Herman–Wallis  $A$  coefficients about an order of magnitude larger than those observed ear-

TABLE I. Intensities, band origins and rotational parameters of the new overtone transitions in HCN, H<sup>13</sup>CN, and HC<sup>15</sup>N. No statistical error bars are given for the intensities, since other sources of error give an effective uncertainty on the order of 10%. The same holds for the band origin values, whose error depends on the calibration procedure and is  $\sim 0.02 \text{ cm}^{-1}$ . The errors for the other parameters are given as two standard deviations. The lower state rotational constants were constrained in the fits to the accurate experimental values (Refs. 3, 5, and 32).

Transition	Intensity cm/mol	Band origin cm <sup>-1</sup>	$\Delta B \times 10^3$ cm <sup>-1</sup>	$\Delta D \times 10^6$ cm <sup>-1</sup>
HCN: $B_0 = 1.478\,221\,62 \text{ cm}^{-1}$ , $D_0 = 2.909\,94 \times 10^{-6} \text{ cm}^{-1}$				
11 <sup>1</sup> 5←010 <sup>b</sup>	3.70(11)	17 449.296	-62.94(14)	0.03(38)
403←000	$3.84(6) \times 10^{-2}$	17 699.376	-70.26(16)	-0.11(40)
11 <sup>e</sup> 5←000 <sup>b</sup>	$1.27(4) \times 10^{-2}$	18 162.762	-63.71(14)	-0.49(34)
11 <sup>f</sup> 5←000 <sup>b</sup>	$1.52(8) \times 10^{-2}$	18 162.748	-55.32(8)	0.19(10)
01 <sup>1</sup> 6←010	2.57(4)	18 255.855	-65.63(8)	-0.05(10)
602←000	$1.53(10) \times 10^{-2}$	18 603.438	-78.9(5)	-0.1(24)
304←000	$9.8(10) \times 10^{-2}$	18 661.368	-72.31(6)	-0.24(10)
21 <sup>1</sup> 5←010	0.47(3)	19 428.022	-70.7(10)	-2.(8)
H <sup>13</sup> CN: $B_0 = 1.439\,995 \text{ cm}^{-1}$ , $D_0 = 2.767\,562\,4 \times 10^{-6} \text{ cm}^{-1}$				
11 <sup>1</sup> 5←010 <sup>b</sup>	–	17 333.724	-58.91(14)	-0.02(42)
105←000	–	17 431.957	-59.85(12)	-0.08(30)
403←000	–	17 534.654	-67.13(36)	-1.1(16)
11 <sup>e</sup> 5←000 <sup>b</sup>	–	18 041.118	-59.67(14)	-0.12(32)
11 <sup>f</sup> 5←000 <sup>b</sup>	–	18 041.114	-51.74(12)	0.27(18)
01 <sup>1</sup> 6←010 <sup>b</sup>	–	18 140.160	-60.94(5)	-0.13(6)
006←000	–	18 257.280	-62.288(28)	-0.087(26)
304←000 <sup>a</sup>	$\geq 4.66 \times 10^{-2}$	18 506.862	-67.94(20)	2.2(5)
72 <sup>0</sup> 1←000 <sup>a</sup>	$\geq 1.5 \times 10^{-2}$	18 512.576	-70.7(6)	2.4(16)
12 <sup>0</sup> 5←000	$\geq 1.9 \times 10^{-2}$	18 636.389	-51.47(12)	4.33(28)
01 <sup>e</sup> 6←000 <sup>b</sup>	$\geq 1.3 \times 10^{-2}$	18 847.496	-61.43(16)	0.1(5)
01 <sup>f</sup> 6←000 <sup>b</sup>	$\geq 1.2 \times 10^{-2}$	18 847.500	-53.96(8)	0.18(10)
205←000	–	19 388.873	-68.69(6)	-0.06(6)
503←000	$\geq 9.1 \times 10^{-3}$	19 477.623	-75.76(42)	1.4(20)
11 <sup>1</sup> 6←010	–	20 087.932	-69.35(36)	0.4(18)
106←000	–	20 206.535	-70.658(28)	-0.06(6)
01 <sup>1</sup> 7←010	–	20 833.220	-72.77(40)	-3.5(12)
007←000	–	20 971.361	-73.728(42)	-0.14(6)
305←000	–	21 325.219	-78.10(12)	-0.31(30)
HC <sup>15</sup> N: $B_0 = 1.435\,248 \text{ cm}^{-1}$ , $D_0 = 2.747\,732\,3 \times 10^{-6} \text{ cm}^{-1}$				
205←000	–	19 459.738	-70.73(6)	0.17(12)
106←000	–	20 301.905	-72.82(12)	-0.09(26)
007←000	–	21 093.192	-76.46(5)	-0.24(10)
305←000	–	21 386.892	-80.27(36)	-0.1(14)
206←000	–	perturbed, see 3 levels fit.		
107←000	–	23 000.358	-84.28(8)	0.01(18)

<sup>a</sup>These two bands are strongly mixed, producing transfer of intensity from the 304 to the 72<sup>0</sup>1 band. Notice also the large “centrifugal distortion” parameter of these bands.

<sup>b</sup>The  $q$   $k$ -doubling parameters for these transitions are reported in Table VII.

lier for the transitions from the ground states to the  $\Sigma$  states (0,0,4) and (0,0,5) [ $A = 0.0014(5)$  and  $-0.0014(3)$ , respectively].<sup>10</sup>

The results of our data analysis are reported in Table I. As explained above, we do not report the intensity of most of the isotopomer bands since the corresponding values for normal HCN are more accurate. Also, we do not list the standard deviations for the intensity data, since the effective experimental reproducibility is much larger, roughly 10%. The same argument holds for the band origins, where the absolute wave number calibration was obtained by observing the optical galvanic effect in a Neon hollow-cathode lamp.<sup>27,28</sup> The accuracy of these calibration lines is of  $\sim 0.02 \text{ cm}^{-1}$ .

From the intensity of the normal isotopomer overtone

bands that appeared in some of our H<sup>13</sup>CN scans, we were able to determine the amount of HCN impurity in the H<sup>13</sup>CN sample. Since we synthesized H<sup>13</sup>CN from isotopically enriched KCN, the impurity derives from the salt. The partial pressure of HCN found from 205, 006, and 105 band spectra appeared in H<sup>13</sup>CN scans, is 8.1, 8.35, and 7.6 torr (out of a total of 100 torr), respectively. To obtain these values, we have used the band intensities determined in our previous work.<sup>16</sup> These values are consistent with the nominal 10% <sup>12</sup>C content of the salt. Even after correction for the presence of this impurity, the band intensities for H<sup>13</sup>CN are consistently smaller than the corresponding values in HCN. This indicates additional impurity levels varying from 10%

TABLE II. Calculated intensities in cm/mol for the over tone transitions in the range 17 500 to 23 000  $\text{cm}^{-1}$ , for the most common isotopomers. As explained in the text, we used the potential by CH&M (Ref. 17) and Botschwina's dipole moment surface (Ref. 19). Experimental values are for HCN, as reported here and in our previous paper (Ref. 16).

State	Experiment	HCN	H <sup>13</sup> CN	HC <sup>15</sup> N
105	3.51	4.32	4.04	4.17
006	2.61	3.15	3.58	3.32
403	0.038	0.049	0.049	0.16
304	0.098	0.14	0.097	0.14
205	0.58	0.66	0.52	0.57
106	0.89	1.15	1.14	1.15
007	0.55	0.55	0.67	0.60
602	0.015	0.018	0.003	0.005
305	0.092	0.099	0.064	0.075
206	0.22	0.28	0.25	0.24
107	0.24	0.30	0.33	0.32

to 30%, if one assumes that the corresponding bands should have the same intensity. The same observation holds for the isotopomer HC<sup>15</sup>N.

To estimate the expected change in band intensity with isotopic substitution, we made intensity calculations using the accurate potential surface recently fitted by CH&M<sup>17</sup> and the *ab initio* dipole moment surface by Botschwina.<sup>19</sup> We used a program<sup>29</sup> that calculates the Hamiltonian matrix on a basis of products of Morse oscillator wave functions for the two bond coordinates. The basis included all bound states with energy expectation value of 60 000  $\text{cm}^{-1}$  (for HCN these are 382 wave functions). A correction was included to account for the bend-stretch coupling to second order. The matrix of eigenvectors was used to transform the dipole moment operator to obtain transition moments from the ground state. The resulting intensity values of the bands of interest for the most common HCN isotopomers are listed in Table II. With a few exceptions, these values compare very favorably with the experimental ones.<sup>16</sup> Even though the isotopic variation is somewhat larger than we had expected, especially for the weaker bands, it is generally smaller than the uncertainties of our H<sup>13</sup>CN and HC<sup>15</sup>N experimental intensities. Further, the calculated values do not show the observed systematic trend of smaller intensities for the H<sup>13</sup>CN and HC<sup>15</sup>N isotopomers. We conclude that the observed lower intensities of these species is due to reduced sample purity and we report only the intensity data of a few H<sup>13</sup>CN bands which we did not already measure in HCN.

The presence of lines due to impurities (likely water and CO<sub>2</sub>) complicated some of our spectra, like the 304←000 and the 403←000 H<sup>13</sup>CN transitions. In these cases we cryotrapped the sample back into its bottle and let it slowly evaporate to refill the RDC, before taking a second scan. Due to the different vapor pressures, we usually obtained cleaner spectra. When the signal/noise allowed, we used spectral subtraction to eliminate the impurity lines (see Fig. 1).

Bands were vibrationally assigned by using the predictions of the variational calculations of CH&M<sup>17,18</sup> which, as shown in Table III, generally predict the observed energy levels to within a few inverse centimeters. For most transitions, the assignments could also be unambiguously made by

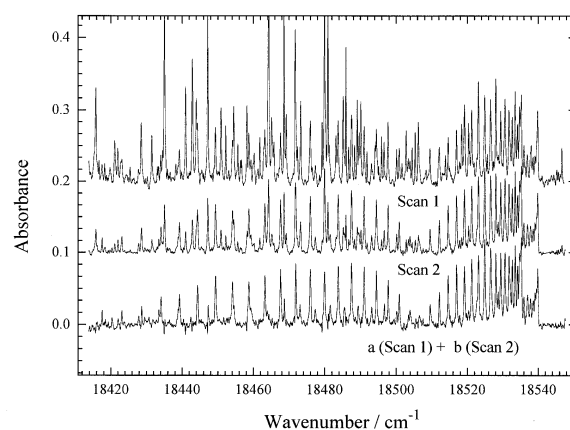


FIG. 1. 304 and 72<sup>0</sup><sub>1</sub> overtone transitions in H<sup>13</sup>CN. Experimental conditions: 100 torr, 60 km absorption path length. Two scans are shown together with a linear combination of the two that removes the spurious lines almost completely.

predictions based upon literature anharmonic constants.<sup>10</sup>

The assignment of some of the weaker overtones was not completely obvious. In H<sup>13</sup>CN, the 304 transition (Fig. 1) appears as two overlapping bands with almost the same origin but quite different rotational spacing. CH&M's calculations predict these to be an almost 50% mixture of the 304 and 72<sup>0</sup><sub>1</sub> states, with some contribution from the 602 state. The rotational fit to these bands is satisfactory (the rms deviation for the combination differences is close to the standard deviation), but gives anomalously large  $\Delta D$  values (see Table I). As an indication of the strength of the mixing we can compare the expected  $\Delta B$  values for the 304 and 72<sup>0</sup><sub>1</sub>

TABLE III. Comparison of the band origins (in  $\text{cm}^{-1}$ ) of the observed  $\Sigma \leftarrow \Sigma$  transitions with values calculated by CH&M.<sup>17,18</sup> The accuracy of the experimental values is 0.02  $\text{cm}^{-1}$ .

State	Experiment	Calculated	Observed-Calculated
HCN:			
403	17 699.376	17 699.88	-0.50
602	18 603.438	18 602.27	+1.16
304	18 661.368	18 660.92	+0.45
H <sup>13</sup> CN:			
105	17 431.957	17 430.78	+1.18
403	17 534.654	17 535.33	-0.68
006	18 257.280	18 255.78	+1.50
304	18 506.862	18 505.73	+1.13
72 <sup>0</sup> <sub>1</sub>	18 512.576	18 510.55	+2.03
12 <sup>0</sup> <sub>5</sub>	18 636.389	18 638.60	-2.21
205	19 388.873	19 387.49	+1.38
503	19 477.623	19 478.03	-0.41
106	20 206.535	20 203.66	+2.88
007	20 971.361	20 968.94	+2.42
305	21 325.219	21 324.23	+0.99
HC <sup>15</sup> N:			
205	19 459.738	19 458.16	+1.58
106	20 301.905	20 298.95	+2.96
007	21 093.192	21 091.17	+2.02
305	21 386.892	21 385.80	+1.09
107	23 000.358	22 995.68	+4.68

states,  $-67.54$  and  $-74.17$  ( $\times 10^{-3} \text{ cm}^{-1}$ ), with those obtained from band fits,  $-67.94$  and  $-70.70$  for the assigned 304 and  $72^0_1$  bands, respectively. The close match would suggest that the mixing of the two states is not as strong as 50%. The regular intensity profile rules out the contribution of Coriolis type interaction, consistent with the  $\Sigma$  symmetry of these states, and supports an anharmonic coupling between them. Finally, if we assume that the  $72^0_1$  band has negligible transition strength compared to the 304, the observed intensity ratio of the bands ( $\sim 1:3$ ), gives the size of the mixing amplitudes, which are roughly  $\sqrt{75\%} = 0.87$  and  $\sqrt{25\%} = 0.50$ , respectively. Combined with the observed splitting of the two levels, we calculate the effective anharmonic matrix element  $\langle 304|H|72^0_1 \rangle = 2.47 \text{ cm}^{-1}$ .

The expected  $\Delta B$  values reported above have been extrapolated from a nonweighted fit involving all  $\Delta B$ 's for previously observed  $\text{H}^{13}\text{CN}$  transitions<sup>29</sup> plus those from our own data, excluding states that are too weak or likely affected by small perturbations. To extend the fit, we had to lock some of the  $\gamma$  parameters, as shown in Table IV, to values obtained from a previous fit done with weights accounting for the expected model errors.<sup>29</sup> This was necessary since the new data tended to destabilize the fit. While this could be a consequence of the lower quality of the added data, it more likely reflects a failure of the anharmonic expansion at these energies, caused by the increasing chance for quasis resonances. HCN has been more thoroughly studied in the mid and near-IR and thus the second order vibration-rotation interaction constants could be determined from fits to lower energy bands.<sup>29</sup> Similarly, we did a nonweighted least-squares fit of the observed  $\Delta B$  values for all the known  $\text{HC}^{15}\text{N}$  bands in order to improve the vibration-rotation interaction constants for this isotopomer. As shown in Table V, due to the limited number of observed bands of this isotopomer, we needed to constrain most of the  $\gamma$  parameters to their HCN values.<sup>29</sup>

In HCN, the 304 state is again perturbed, but mainly by the 602 state. This is a case of the 3-2 anharmonic resonance between modes  $\nu_1$  and  $\nu_3$  that appears sporadically throughout the HCN overtone spectrum.<sup>30,31</sup> The band origins for the 304 and 602 states, are  $58 \text{ cm}^{-1}$  away. For these states, we do not even find unusually large  $\Delta D$  values. Assuming that most of the 602 transition intensity is due to the mixing, from the intensity ratio we obtain the mixing amplitudes 0.93 and 0.37 for the 304 and 206 states, respectively, implying a matrix element  $\langle 304|H|206 \rangle = 29.9 \text{ cm}^{-1}$ .

In the fitting of a complex spectrum, it is extremely valuable to predict anharmonic matrix elements by scaling formulas based upon harmonic oscillator matrix elements of the lowest order that can couple the two states. For example, we have

$$W = \langle \nu_1, \nu_2, \nu_3 | H | \nu_1 + 3, \nu_2, \nu_3 - 2 \rangle \\ = K_{111;33} \sqrt{(\nu_1 + 1)(\nu_1 + 2)(\nu_1 + 3)\nu_3(\nu_3 - 1)}, \quad (1)$$

where  $K_{111;33}$  would be constant for all cases of interaction with the same form. Little is known about the accuracy of such scaling laws, especially at high energy. With the present results, there are now four examples of the 3-2 resonance

TABLE IV. Fit of  $\Delta B$ 's for all known overtone states in  $\text{H}^{13}\text{CN}$ . Calculated using  $B_0 = 1.439\,992(2) \text{ cm}^{-1}$ . Equal data weighting was used. Some of the values have been obtained from a hot band by adding the known  $\Delta B$  of one of the states in the transition. All values are in units of  $10^{-3} \text{ cm}^{-1}$ . Errors are given as two standard deviations. Locked parameters are from a previous fit done on HCN with a special model weighting (Ref. 29).

State	$\Delta B/10^{-3} \text{ cm}^{-1}$	Fit	Obs.-Calc.	Ref.
01 <sup>1</sup> 0	3.221	3.204	0.017	35,36
11 <sup>1</sup> 0	-6.696	-6.624	-0.072	37
02 <sup>0</sup> 1	-3.09	-3.065	-0.025	6
02 <sup>2</sup> 1	-2.79	-2.765	-0.025	6
02 <sup>0</sup> 0	6.4691	6.419	0.050	38
02 <sup>0</sup> 0	6.1603	6.119	0.042	38
01 <sup>1</sup> 1	-6.2168	-6.204	-0.013	38
001	-9.6283	-9.633	0.005	38
101	-19.186	-19.102	-0.084	6
01 <sup>1</sup> 2	-15.928	-15.909	-0.019	6
002	-19.5449	-19.563	0.018	39
01 <sup>1</sup> 2	-15.949	-15.909	-0.040	6
102	-28.919	-28.853	-0.066	39
003	-29.7620	-29.790	0.028	39
103	-38.880	-38.901	0.021	40
005	-51.1537	-51.135	-0.019	41
303	-57.456	-57.591	0.135	41
204	-58.3883	-58.333	-0.055	41
105	-59.8674	-59.887	0.020	41
006	-62.300	-62.253	-0.047	41
11 <sup>1</sup> 5	-55.697	-55.739	0.042	
01 <sup>1</sup> 6	-57.695	-57.699	0.004	
403	-67.13	-67.171	0.041	
205	-68.687	-68.796	0.109	
106	-70.658	-70.826	0.168	
007	-73.728	-73.668	-0.060	
305	-78.095	-77.861	-0.234	

Fit model:

$$B_v = B_e - \sum \alpha_i(n_i + d_i/2) + \sum_{i>j} \gamma_{ij}(n_i + d_i/2)(n_j + d_j/2) + \gamma_{\ell\ell\ell} \ell^2$$

Fit results/ $10^{-3} \text{ cm}^{-1}$

$$\begin{array}{lll} \alpha_1 = -9.40(16) & \gamma_{11} = -0.0789(26) & \gamma_{12} = -0.180(\text{locked}) \\ \alpha_2 = -3.317(54) & \gamma_{22} = -0.070(\text{locked}) & \gamma_{23} = -0.224(28) \\ \alpha_3 = -9.650(68) & \gamma_{33} = -0.149(8) & \gamma_{13} = -0.180(24) \\ & \gamma_{\ell\ell\ell} = -0.075(\text{locked}) & \end{array}$$

Standard deviation =  $8.7 \times 10^{-5} \text{ cm}^{-1}$

known in HCN. Using the relative intensities (which are not affected by errors due to sample purity) and the observed splitting, we can calculate effective coupling matrix elements. These are shown in Table VI. We see that except for the lowest member of the progression, the agreement with the scaling formula is within a few percent. The lowest member has the weakest mixing of the levels, and thus for this case the assignment of negligible intrinsic intensity for the  $|3,0,2\rangle$  state may be responsible for the overestimate of the matrix element.

The assignments of transitions such as  $01^1_6 \leftarrow 000$ , could be checked against the hot bands with the same upper state, like  $01^1_6 \leftarrow 01^1_0$ . In all cases the rotational constants of the upper state match within the experimental error. Also the values of  $q$  derived both from the combination band and from the corresponding hot band are in good agreement (see Table VII). With respect to the band origins, in  $\text{H}^{13}\text{CN}$  the hot-cold band difference matches the known bend fundamental frequency within the experimental errors, while in

TABLE V. Fit of  $\Delta B$ 's for all known overtone states in  $\text{HC}^{15}\text{N}$ . Calculated using  $B_0=1.435\,249(2)\text{ cm}^{-1}$  (Ref. 3). Equal data weighting was used. Some of the values have been obtained from a hot band by adding the known  $\Delta B$  of one of the states in the transition. All values are in units of  $10^{-3}\text{ cm}^{-1}$ . Errors are given as two standard deviations. Locked parameters are from a previous fit done on HCN with a special model weighting (Ref. 29).

State	$\Delta B/10^{-3}\text{ cm}^{-1}$	Fit	Obs.–Calc.	Ref.
01 <sup>1</sup> 0	3.391	3.347	0.045	35,36
11 <sup>1</sup> 0	-6.380	-6.285	-0.095	37
01 <sup>1</sup> 1	-6.405	-6.456	0.051	38
001	-10.0043	-10.017	0.013	38
002	-20.3050	-20.321	0.016	39
003	-30.888	-30.912	0.024	39
005	-53.0722	-52.954	-0.118	41
303	-58.2241	-58.436	0.212	41
204	-59.6113	-59.809	0.198	41
105	-61.7473	-61.799	0.051	41
006	-64.5829	-64.406	-0.177	41
205	-70.726	-70.714	-0.012	
106	-72.82	-73.120	0.300	
007	-76.46	-76.144	-0.316	
305	-80.27	-79.700	-0.570	
107	-84.284	-84.729	-0.445	

Fit model:

$$B_v = B_e - \sum \alpha_i (n_i + d_i/2) + \sum_{i>j} \gamma_{ij} (n_i + d_i/2)(n_j + d_j/2) + \gamma_{\ell\ell} \ell^2$$

Fit results/ $10^{-3}\text{ cm}^{-1}$

$$\begin{array}{lll} \alpha_1 = -9.35(44) & \gamma_{11} = -0.0353(\text{locked}) & \gamma_{12} = -0.1373(\text{locked}) \\ \alpha_2 = -3.36(34) & \gamma_{22} = 0.0503(\text{locked}) & \gamma_{23} = 0.2145(\text{locked}) \\ \alpha_3 = 10.01(20) & \gamma_{33} = -0.143(28) & \gamma_{13} = 0.13(10) \\ & \gamma_{\ell\ell} = -0.201\,83(\text{locked}) & \end{array}$$

$$\text{Standard deviation} = 2.8 \times 10^{-4}\text{ cm}^{-1}$$

HCN we actually had to use the bend fundamental to calibrate the  $11^15 \leftarrow 01^10$  band since we did not have calibration lines in the region scanned while we did for the corresponding cold band.

Rotational fits for  $\Sigma \leftarrow \Sigma$  transitions were done using the model

TABLE VI. Analysis of the scaling law for  $\langle n, 0, 4 | H | n + 3, 0, 2 \rangle$  interactions. From properties off a  $2 \times 2$  matrix, if all intensity comes from one of the two basis functions,  $|W| = |\Delta E| \sqrt{I_1 I_2} / (I_1 + I_2)$ . The values for  $K_{111;33}$  have been calculated using Eq. (1).

State	Band origin $\text{cm}^{-1}$	Intensity $\text{cm}/\text{mol}$	$ W $ $\text{cm}^{-1}$	$K_{111;33}$ $\text{cm}^{-1}$
004	12 635.888	157.0(10)		
302	12 657.8763	9.11(25)	5.01(6)	0.590(7)
104	14 670.447	9.42(9)		
402	14 653.660	8.33(10)	8.378(4)	0.4937(2)
204	16 674.211	1.7(1)		
502	16 640.313	0.40(4)	13.3(5)	0.496(18)
304	18 661.368	0.098(1)		
602	18 603.438	0.015(1)	19.6(4)	0.516(10)

TABLE VII. Values of the  $q$   $K$ -doubling parameter for some  $\Pi$  states. Errors are given as twice the standard deviations. The two values derived from the hot bands are obtained by fitting the model in Eq. (4) to the resolved splittings, with  $q''$  fixed to the literature values of  $1.871\,933$  and  $1.769(8) \times 10^{-3}\text{ cm}^{-1}$  for HCN and  $\text{H}^{13}\text{CN}$  respectively (Ref. 32 and 6).

State	$q'/10^{-3}\text{ cm}^{-1}$	Source
HCN:		
11 <sup>1</sup> 5	2.09(4)	11 <sup>1</sup> 5 $\leftarrow$ 000
H <sup>13</sup> CN:		
11 <sup>1</sup> 5	1.98(5)	11 <sup>1</sup> 5 $\leftarrow$ 000
11 <sup>1</sup> 5	1.948(10)	11 <sup>1</sup> 5 $\leftarrow$ 01 <sup>1</sup> 0
01 <sup>1</sup> 6	1.87(5)	01 <sup>1</sup> 6 $\leftarrow$ 000
01 <sup>1</sup> 6	1.865(5)	01 <sup>1</sup> 6 $\leftarrow$ 01 <sup>1</sup> 0

$$\begin{aligned} \nu(J) = \nu_0 + (2B'' + \Delta B)m + (\Delta B - \Delta D)m^2 \\ - 2(2D'' + \Delta D)m^3 - \Delta Dm^4 \end{aligned} \quad (2)$$

where  $m$  is the same as defined before. This model derives from the usual term values  $E(J) = E_0 + B[J(J+1) - \ell^2] - D[J(J+1) - \ell^2]^2$ . In this case as in the following ones, the lower state rotational constants were kept locked in the fit to the accurately known experimental values<sup>3,5,6,32</sup>

For  $\Pi \leftarrow \Pi$  transitions (hot bands), we could not resolve the  $Q$  branch and the  $\ell$ -type splitting except for relatively large  $J$  values. For those doublets that could be resolved, we used the center of the doublet. The fitting model is

$$\begin{aligned} \nu(J) = \nu_0 - \Delta B - \Delta D + (2B'' + \Delta B + 4D'' + 2\Delta D)m \\ + (\Delta B + \Delta D)m^2 - 2(2D'' + \Delta D)m^3 - \Delta Dm^4. \end{aligned} \quad (3)$$

For two hot bands enough doublets could be resolved to allow fitting the splitting to the model

$$\Delta \nu(J) = 4(q' + q'')m + 4(q' - q'')m^2, \quad (4)$$

with the results listed in Table VII. This model derives from  $E^\pm(J) = E_0 + B[J(J+1) - 1] - D[J(J+1) - 1]^2 \pm q(\nu_{\text{bend}} + 1)J(J+1)$ . Centrifugal corrections to the  $q$ 's were found not to be significantly different from zero when included in the fits.

For  $\Pi \leftarrow \Sigma$  transitions the  $P$  and  $R$  branches involve the  $e$  sublevels, while the  $Q$  branch involves only the  $f$  sublevels. The term values given above, with  $\ell = 1$  for the  $\Pi$  state, give the fitting models for the  $R$  and  $P$  branches

$$\begin{aligned} \nu(J) = \nu_0 - B'' - \Delta B_e - D'' - \Delta D_e + (2B'' + \Delta B_e + 2D'' \\ + 2\Delta D_e)m + (\Delta B_e + 2D'' + \Delta D_e)m^2 \\ - 2(2D'' + \Delta D_e)m^3 - \Delta D_e m^4, \end{aligned} \quad (5)$$

and for the  $Q$  branch

$$\begin{aligned} \nu(J) = \nu_0 - B'' - \Delta B_f - D'' - \Delta D_f + (\Delta B_f + 2D'' \\ + 2\Delta D_f)J(J+1) - \Delta D_f [J(J+1)]^2. \end{aligned} \quad (6)$$

From the difference of the rotational constants of the  $e$  and  $f$  levels we obtain  $q = (B_e - B_f)/4$ , whose values are also listed in Table VII.

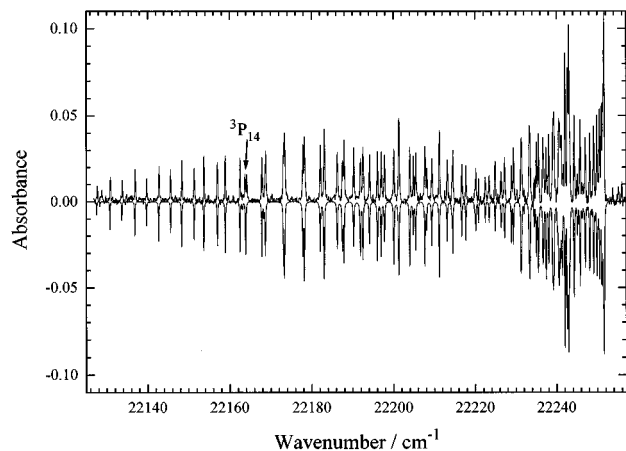


FIG. 2. 206 overtone transition in  $\text{H}^{13}\text{CN}$  feet-to-feet with simulation from fit using the three-level model number 4 (see text). Experimental conditions: 100 torr, 18 km absorption path length.

In each fitted band, we checked for the presence of weak rovibrational perturbations by comparing the standard deviation of the observed and calculated ground state combination differences with the standard deviation of the fit. Since the combination differences are not sensitive to perturbations of the upper level, their standard deviation is a reference value for the wave number precision of the data. In no cases was the fit standard deviation significantly larger than that of the ground state combination differences. Thus we conclude that the effect of local (heterogeneous) perturbations, which result from the crossing of vibrational levels as a function of  $J$ , shift the observed energy levels by an amount no greater than our experimental precision.

### The perturbed 206 system in $\text{HC}^{15}\text{N}$

A low resolution [ $0.2 \text{ cm}^{-1}$  full width at half maximum (FWHM)] overview of the spectrum of the 206 band in  $\text{HC}^{15}\text{N}$  is shown in Fig. 2, foot to foot with a simulation from a fit based on model 4, as described below. A high resolution scan was also taken to partially resolve the many blended lines. The Lambda-Physik FL-2002 dye laser we employed for this measurements allows a  $0.1 \text{ cm}^{-1}$  FWHM resolution when operated with an intracavity etalon.

Initial assignments were made by searching for ground state combination differences. This demonstrated that the spectrum consists of three  $J$  progressions. In Fig. 3 we show a reduced energy plot of upper state term values for the assigned transitions. A  $J$ -dependent offset  $BJ(J+1)$  ( $B=1.3532 \text{ cm}^{-1}$ ) has been subtracted to make the rotational progressions more apparent. It is evident that there is strong interaction, the three progressions getting closer at higher  $J$ 's with an avoided crossing around  $J=17$ . At high  $J$ , the intensity of the middle progression dies out. Only one “bright state” (206) is expected in this spectral region, and anharmonic mixing is responsible for the transition intensity of the other two states.

It can be seen that band 3 (as labeled in Fig. 3) has a small energy jump between  $J=13$  and 14. Correspondingly, in the spectrum we find that the  $P(14)$  and  $R(12)$  lines of

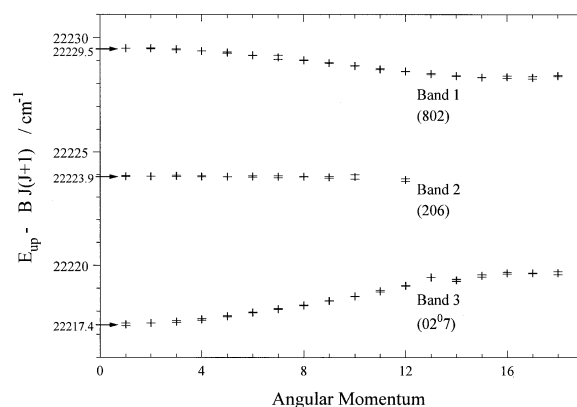


FIG. 3. Reduced energy plot of upper state term values for the assigned transitions in the perturbed 206 band in  $\text{HC}^{15}\text{N}$ . A  $J$ -dependent offset  $BJ(J+1)$  (with  $B=1.3532 \text{ cm}^{-1}$ ) has been subtracted to make the rotational progressions more apparent.

band 3 are both split into doublets (see Fig. 2). We attribute this to a fourth “dark state” whose energy dependence on  $J$  is fast with respect to the size of its coupling with state 3. This perturbation appears to be very localized and will be ignored in the following.

The effective Hamiltonian model that we employed to fit the observed spectrum was chosen to have Anharmonic ( $J$ -independent) coupling between states with the same  $J$

$$H(J) = \begin{bmatrix} E_1(J) & V_{12} & V_{13} \\ V_{12} & E_2(J) & V_{23} \\ V_{13} & V_{23} & E_3(J) \end{bmatrix} \quad (7)$$

where  $E_i(J) = E_{i0} + B_i J(J+1)$ , possibly with higher order terms in  $J(J+1)$ . Parameters of the fit are the  $B_i$ , the band origins  $\nu_i$  and the coupling matrix elements  $V_{ij}$ . The fact that all three bands could be followed down to low  $J$ , with more or less constant relative intensities, confirms that the three states are not connected by  $J$ -dependent Coriolis coupling, consistently with their assignment as  $\Sigma$  states.

We initially fit the observed energies of the upper state, obtained from our assigned spectrum, constraining the accurately known ground state rotational parameters.<sup>3</sup> This fit required calculating the eigenvalues of  $H(J)$  for each  $J$ . The core of the fitting program was the IMSL nonlinear least-square fitting routine ZXSSQ,<sup>25</sup> the same used for all the spectral line fitting. At the end of the fit, the projection coefficients of the eigenstates of the interaction Hamiltonian onto the zero order basis states were given by the eigenvectors of  $H(J)$ . By assuming that only one of the three zero order states has a non zero dipole moment matrix element with the vibrational ground state, the squares of the projection coefficients on this state are proportional to the relative intensities of the three transitions for each  $J$ . A realistic simulation of the spectrum was done by including the rotational Hönl–London factors, the Boltzmann population factor of the lower state and a  $J$ -dependent pressure broadening (empirical fitted modified exponential gap (MEG) law as in Ref. 33). The effects of pressure shifts are expected to be negligible.<sup>7</sup> While the line positions were reproduced fairly

TABLE VIII. Fits of 206 band in  $\text{HC}^{15}\text{N}$  by a three levels model. All parameters of fit are in units of  $\text{cm}^{-1}$ . The frequency data points were 50, while the projection coefficients derived from the relative intensities were 45. See the text for details about the fitting models used. In these fits,  $B_0=1.435\,248\text{ cm}^{-1}$  and  $D_0=2.747\,732\,3\times 10^{-6}\text{ cm}^{-1}$  (Ref. 3).

Model	1	2	3	4
Frequency Pts	50	50	50	50
Projection Pts	0	0	45	45
Freq. rms	0.037	0.015	0.055	0.022
Proj. rms	–	–	0.078	0.073
$\nu_1$	22 227.30	22 227.74	22 227.38	22 227.57
$\nu_2$	22 225.23	22 223.30	22 224.05	22 223.59
$\nu_3$	22 217.73	22 219.09	22 218.87	22 218.99
$\Delta B_1$	$-98.54\times 10^{-3}$	$-95.39\times 10^{-3}$	$-95.71\times 10^{-3}$	$-97.55\times 10^{-3}$
$\Delta B_2$	$-78.20\times 10^{-3}$	$-81.88\times 10^{-3}$	$-83.97\times 10^{-3}$	$-79.87\times 10^{-3}$
$\Delta B_3$	$-69.13\times 10^{-3}$	$-64.01\times 10^{-3}$	$-66.90\times 10^{-3}$	$-64.52\times 10^{-3}$
$V_{12}$	2.72	0.41	2.87	2.77
$V_{23}$	2.09	3.70	0.16	0.32
$V_{13}$	-0.36	2.19	3.20	3.33
$D_1$	–	$0.66\times 10^{-5}$	–	$-0.25\times 10^{-5}$
$D_2$	–	$0.17\times 10^{-5}$	–	$0.95\times 10^{-5}$
$D_3$	–	$1.1\times 10^{-5}$	–	$0.96\times 10^{-5}$

well by this fit, direct comparison with the observed spectrum made it clear that the correct band intensity profile was not reproduced. This was true whatever choice we made for the bright state. Inclusion of a  $D_i[J(J+1)]^2$  term in the  $E_i(J)$  expansion improved the standard deviation by a factor 2, making it the same size as the experimental error, but still produced unacceptable line intensities. Final parameter values and statistics of these fits are reported in the first and second column of Table VIII.

In order to improve the fit, we decided to include information contained in the relative line intensities. For each  $J$ , we divided the intensities of all the assigned  $R(J-1)$  and  $P(J+1)$  lines by the appropriate population factors of the initial state and by the rotational Hönl–London factors. Only lines that were not strongly blended were considered. This would give the “vibrational” intensity for all the corresponding upper levels. For some values of  $J$ , where the intensities of each of the three components could be determined, the sum of these would give the nonfractionated vibrational intensity of the 206 transition. We averaged total vibrational intensity over these values of  $J$ , and then we used it to normalize the intensities of all the states we considered. In this way, we obtained experimental values for the square of the projection coefficient of each rovibrational level on the bright state level belonging to the same  $J$ , which could be directly included in the fitting procedure. Due to faster convergence, the fitting time actually decreased, despite the almost doubled number of fit data. This fact indicates that the inclusion of the intensity information breaks strong correlations among the parameters of the model, responsible for a sluggish convergence to an incorrect solution. The results and statistics for this fit are in column 3 of Table VIII, while column 4 gives the results of a fit which also includes the  $D_i$  parameters. In the table, we separately give rms deviations of the frequency and of the intensity data points. It can be seen that the inclusion of the distortion terms  $D_i$  signifi-

cantly improves the fit, especially with respect to the frequencies. Without  $D_i$  terms, we also tried to include in the coupling coefficients terms of the form  $V'_{ij}J(J+1)$ , with results comparable to the last fit model. These variations to the model give an estimate of how stable the  $B$  and  $V_{ij}$  values are if one introduces higher order terms in the effective Hamiltonian.

In these last fits, the bright state was chosen to be the middle state 2. It is interesting that the inclusion of the intensity information gives the fit a strong convergence property, which virtually allows for an automatic assignment of the bright state. In fact, using the same initial conditions, but assigning bright state character to any one of the zero order states, the fits converge always to the same solution, but with a different correspondence of the diagonal states to the zero-order states, such that the closest to the bright state is again the middle one. This also assures us that no other assignment would lead to a correct reproduction of the experimental spectrum.

In the least-squares fit to both line positions and mixing coefficients, some relative weight factor for this two independent data sets must be used in the definition of the  $\chi^2$ . In the present case, the relative error in the line frequencies,  $\sim 0.01\text{ cm}^{-1}$ , nearly matched that of the mixing coefficients,  $\sim 2\%$ , and therefore we could use a weight factor of 1. We found that if we weighted the frequency some 50% more than the mixing coefficients, or the other way round, the result of the fit would be unacceptable either for the intensities or for the frequencies, respectively.

As mentioned earlier, we used “parameter toggling” to make the fit more robust. In fact, if one tries to fit all the parameters in  $H(J)$  simultaneously, the fit will not converge, even for good choices of the initial values. This is a problem often found in nonlinear least squares fits plagued by high levels of correlation among the parameters. By grouping the

parameters so that inside each group the correlations are smaller, it is possible to make the fit converge with respect to variations of these parameters alone. These best fit parameters are then frozen while the next group of parameters is varied, and the cycle repeated until convergence. In the present case, we found that we could get stable convergence by putting into one group all the  $J$  independent parameters (that is,  $\{\nu_i, V_{ij}\}$ ), and all the remaining ones into another group. Depending on the fit model this second group was  $\{B_i\}$  or  $\{B_i, D_i\}$  or  $\{B_i, V'_{ij}\}$ . A disadvantage of this technique is that it is more involved to obtain the standard errors, since the Jacobian matrix at the converged point in the full parameter space has to be evaluated separately at the end. Since in our case the standard errors are certainly smaller than variations due to changes in the Hamiltonian model (i.e., model errors), we did not calculate them.

The above analysis demonstrates that this region of the absorption spectrum of  $\text{HC}^{15}\text{N}$  is dominated by transitions to three interacting  $\Sigma$  states. We now turn to the results of the variational calculations of CH&M<sup>17,18</sup> to try and assign the normal mode character of these states. Based upon the absence of bend-stretch perturbations throughout the spectrum, we expect the basis states to contain little or no bending excitation. Within a  $30\text{ cm}^{-1}$  region about the observed bands, only three such  $\Sigma$  states are predicted, with band origins at  $22\,230.65$ ,  $22\,224.23$ , and  $22\,218.05\text{ cm}^{-1}$ . These states were assigned as  $02^07$ ,  $802$ , and  $206$ , respectively. Comparison of the experimental band origins (which can be read from Fig. 3) with these predicted values is strikingly good. Notice that these “observed” values are further separated than the zero-order fitted band origins (Table VIII) since they refer to the eigenstates, which are pushed apart by the anharmonic interactions.

The spectroscopic constants of our fits supports the assignment of the absorption features to these three states, but not in the order predicted. As discussed above, our model requires the zero order intensity to be given to the middle of the three zero order states, and based upon the principal isotopomer, we expect the dominant transition strength to come from the  $206$  state. Further support for reassignment comes from the extrapolated  $\Delta B$ 's for the states  $802$ ,  $206$ , and  $02^07$  (using the expansion in Table V), which are  $-96.2$ ,  $-81.9$ , and  $-65.9 \times 10^{-3}\text{ cm}^{-1}$ , respectively. Comparison of the fitted  $\Delta B$ 's from Table VIII shows excellent agreement if we assign the states  $802$ ,  $206$ , and  $02^07$  to states  $1$ ,  $2$ , and  $3$ , respectively. Lastly, the coupling coefficients derived from the fit further support this assignment. The anharmonic couplings between states  $2-1$  and  $2-3$  are substantially larger than the  $1-3$  coupling. This is consistent with a simple consideration of the total number of quanta that the interaction operator has to exchange to connect state  $1$  ( $206$ ) with  $2$  ( $802$ ) ( $10$  stretching quanta),  $2$  with  $3$  ( $02^07$ ) ( $5$  stretching and  $2$  bending), and  $1$  with  $3$  ( $15$  stretching and  $2$  bending). Given the weakness of the bend-stretch coupling in HCN, it is reasonable that a fifth order interaction that mixes in the bending mode could be of the same size as a eight order matrix element that couples only stretching modes.

The difference in the assignment is not due to comparison of the results of the deperturbation with the eigenstates

predicted by the variational calculation. At low  $J$ , the mixing of the three states is not dramatic, and the dominant character of the eigenstates is that of the nearest basis state. For example, the  $J=0$  projection amplitudes of the middle state on the zero-order states  $1$ ,  $2$ , and  $3$  are, in the order,  $-0.3006$ ,  $0.9335$ , and  $-0.1955$ .

The assignments of HC&M are based upon the maximum overlap of the eigenfunctions with the basis functions that were used in the final diagonalization. However, as they pointed out to us, the basis they use in the final diagonalization is already a contraction of the original product basis, and thus could be strongly “renormalized” by interactions already treated in earlier diagonalizations. Further, it must be remembered that it is extremely difficult to assign unambiguous quantum numbers in a multidimensional system, and at this energy, HC&M remarked that their program gave many duplicate assignments. However, the  $\Delta B$  values calculated by HC&M for the states they assign as  $206$ ,  $802$ , and  $02^07$  respectively, are  $-79$ ,  $-87$ , and  $-50$  ( $\times 10^{-3}\text{ cm}^{-1}$ ), and compared with the extrapolated values given before are quite consistent with the assignment by their program. In conclusion, the states predicted by HC&M are not as close to the observed ones as it seems at a first glance, since indeed their ordering is incorrect.

The specific values for  $\Delta B$  calculated by HC&M cannot be directly compared with those in Table VIII since their values are calculated from the rotational energy dependence (between  $J=0$  and  $1$ ) of the eigenstates, while our values are for the deperturbed basis states. The average (over the three states) can be compared since the perturbations should not effect the average energy at each  $J$ .  $\Delta B$  for the three states is calculated by HC&M as  $-72. \times 10^{-3}\text{ cm}^{-1}$  while our analysis gives  $-81. \times 10^{-3}\text{ cm}^{-1}$ . This level of agreement is consistent with the accuracy of HC&M's predicted rotational constants for unperturbed stretching states in the same energy region, where they consistently predict rotational constants slightly too large.

#### IV. CONCLUSION

The present paper extends our earlier study of the overtone spectrum of HCN, using the method of cavity ring down spectroscopy. We have reported numerous bands of the two minor isotopomers of HCN.

Variational calculations on the empirical potential of CH&M does an excellent job of predicting these observed band positions, including isotopic shifts. In the one observed case of an extensively perturbed band system, with three strongly interacting levels, the empirical potential accurately predicts the three states that are interacting, as shown by the deperturbed rotational constants and qualitatively by the size of the three interaction matrix elements. Although the observed  $J=0$  levels splittings are also accurately predicted by theory, the zero order assignment of the levels does not agree with our deperturbation of the observed spectrum. Despite this one failing, the observed spectra strongly reinforce the accuracy of this empirical potential up to the highest observed levels of HCN. By extension, the variational method of force field refinement is demonstrated to be the best available method for determining potential energy surfaces from

experimental data, at least for triatomics for which converged variational calculations are “cheap” enough to allow their inclusion in a least squares fitting package.

While, due to problems of sample purity, most of the band intensities could not be measured accurately except for the principal isotopomer, the intensities that were determined are in agreement with predictions based on Botschwina’s dipole moment surface. It should be noted that the overtone intensities are significantly more accurately predicted by the new CCSD(T)<sup>19</sup> calculations compared with the earlier coupled electron pair approximation (CEPA) calculations (also by Botschwina<sup>34</sup>). The observed perpendicular bands of HCN are found to be much weaker than the parallel bands, and show evidence of Herman–Wallis effects likely due to Coriolis mixing with states responsible for the much stronger parallel bands. We are currently working on a calculation of Herman–Wallis effects in HCN combining a simplified two dimensional variational treatment of the vibrational wave functions (treating the bending mode as harmonic) with a perturbation treatment of vibration–rotation interactions. We will report on this work at a later time.

The present results, combined with recent work in other laboratories, demonstrates that HCN continues to be an important model system for testing the highest levels of theory. In a future publication, we will present results for a study of pressure broadening and line mixing in HCN, studied once again by the CRDS method. This work, combined with recent state-to-state inelastic collisional measurements will provide a challenge to the theory of molecular collisions as well.

## ACKNOWLEDGMENTS

We would like to thank Dr. Stuart Carter, Dr. Ian Mills, and Dr. Peter Botschwino for providing us with their unpublished results. This work was supported by the National Science Foundation.

<sup>1</sup>K. K. Lehmann and A. M. Smith, *J. Chem. Phys.* **93**, 6140 (1990).

<sup>2</sup>D. H. Rank, G. Skorinko, D. P. Eastman, and T. A. Wiggins, *J. Opt. Soc. Amer.* **50**, 421 (1960).

<sup>3</sup>G. Winnewisser, A. G. Maki, and D. R. Johnson, *J. Mol. Spectrosc.* **39**, 149 (1971).

<sup>4</sup>A. G. Maki, *J. Mol. Spectrosc.* **58**, 308 (1975).

<sup>5</sup>J. I. Choe, T. Tipton, and S. G. Kukolich, *J. Mol. Spectrosc.* **117**, 292 (1986).

<sup>6</sup>K. K. Lehmann, G. J. Scherer, and W. Klemperer, *J. Chem. Phys.* **77**, 2853 (1982).

<sup>7</sup>A. M. Smith, K. K. Lehmann, and W. Klemperer, *J. Chem. Phys.* **85**, 4958 (1986).

<sup>8</sup>A. M. Smith, U. G. Jørgensen, and K. K. Lehmann, *J. Chem. Phys.* **87**, 5649 (1987).

<sup>9</sup>A. M. Smith, W. Klemperer, and K. K. Lehmann, *J. Chem. Phys.* **90**, 4633 (1989).

<sup>10</sup>A. M. Smith, S. L. Coy, W. Klemperer, and K. K. Lehmann, *J. Mol. Spectrosc.* **134**, 134 (1989).

<sup>11</sup>H. Sasada, *J. Chem. Phys.* **88**, 767 (1988).

<sup>12</sup>X. Yang, C. A. Rogaski, and A. M. Wodtke, *J. Chem. Phys.* **92**, 2111 (1990).

<sup>13</sup>X. Yang, C. A. Rogaski, and A. M. Wodtke, *J. Opt. Soc. B* **7**, 1835 (1990).

<sup>14</sup>X. Yang and A. M. Wodtke, *J. Chem. Phys.* **93**, 3723 (1990).

<sup>15</sup>J. Wu, R. Huang, M. Goup, A. Soury, E. Carrasquillo M., *J. Chem. Phys.* **99**, 6474 (1993).

<sup>16</sup>D. Romanini and K. K. Lehmann, *J. Chem. Phys.* **99**, 6287 (1993).

<sup>17</sup>S. Carter, I. M. Mills, and N. C. Handy, *J. Chem. Phys.* **99**, 4379 (1993).

<sup>18</sup>I. M. Mills (private communication).

<sup>19</sup>P. Botschwina, B. Schulz, M. Horn, and M. Matuschewski, *Chem. Phys.* (to be published).

<sup>20</sup>N. Jacobi and J. H. Jaffe, *J. Mol. Spectrosc.* **10**, 1 (1963).

<sup>21</sup>C. di Lauro and I. M. Mills, *J. Mol. Spectrosc.* **21**, 386 (1966).

<sup>22</sup>A. G. Maki, S. Klee, G. Mellau, and W. Quapp, *Ohio State University International Symposium on Molecular Spectroscopy* (T. A. Miller, Department of Chemistry, Ohio State University, Columbus, Ohio, 1993).

<sup>23</sup>A. O’Keefe and D. A. G. Deacon, *Rev. Sci. Instrum.* **59**, 2544 (1988).

<sup>24</sup>R. Lalezari (private communication).

<sup>25</sup>*IMSL FORTRAN library, Vol.4, Routine ZXSSQ*, 9.0 ed., IMSL, Houston, 1982.

<sup>26</sup>J. K. G. Watson, *J. Chem. Phys.* **153**, 211 (1992).

<sup>27</sup>W. Demtröder, *Laser Spectroscopy*, 2nd ed. (Springer-Verlag, Berlin, 1982).

<sup>28</sup>*M.I.T. Wavelength Tables* (MIT Press, Cambridge, Massachusetts, 1982).

<sup>29</sup>A. M. Smith, Ph.D. thesis, Harvard University, Cambridge, MA, 1988.

<sup>30</sup>A. E. Douglas and D. Sharma, *J. Chem. Phys.* **21**, 445 (1952).

<sup>31</sup>H. C. Allen, E. D. Tidwell, and E. K. Plyler, *J. Chem. Phys.* **25**, 302 (1956).

<sup>32</sup>S. Paddi Reddy, W. Ivancic, V. Malathy Devi, A. Baldacci, K. Narahari Rao, A. W. Mantz, *R. S. Eng. Appl. Opt.* **18**, 1350 (1979).

<sup>33</sup>A. S. Pine and J. P. Looney, *J. Chem. Phys.* **96**, 1704 (1992).

<sup>34</sup>P. Botschwina, *J. Chem. Soc. Faraday Trans. 2* **84**, 1263 (1988).

<sup>35</sup>T. Nakagawa and Y. Morino, *Bull. Chem. Soc. Jap.* **42**, 2212 (1969).

<sup>36</sup>M. L. Sage and J. Jortner, *Adv. Chem. Phys.* **47**, 293 (1981).

<sup>37</sup>M. Herbelin and G. Emanuel, *J. Chem. Phys.* **60**, 689 (1974).

<sup>38</sup>R. Deleon and J. Muentner, *J. Chem. Phys.* **80**, 3992 (1984).

<sup>39</sup>J. C. Light and Z. Bačić, *J. Chem. Phys.* **87**, 4008 (1987).

<sup>40</sup>W. Greenlay and B. Henry, *J. Chem. Phys.* **69**, 82 (1978).

<sup>41</sup>E. Heller, *Chem. Phys. Lett.* **61**, 583 (1979).